Hard-edge ICOOL model of the Balbekov square cooling ring

R.C. Fernow
Brookhaven National Laboratory
8 October 2002

We have made a hard-edged ICOOL simulation of Valeri Balbekov's four-sided cooling ring, which was originally designed as a possible test configuration for the MUCOOL experiment. We find a cooling merit factor of 103 after 15 turns.

1. Introduction

Valeri Balbekov was one of the earliest proponents for using ring coolers [1]. The four-sided cooling ring [2] presented at PAC2001 was a particularly elegant solution, which led to the investigation of many alternative ring designs. The layout of the Balbekov ring is shown in Fig. 1.

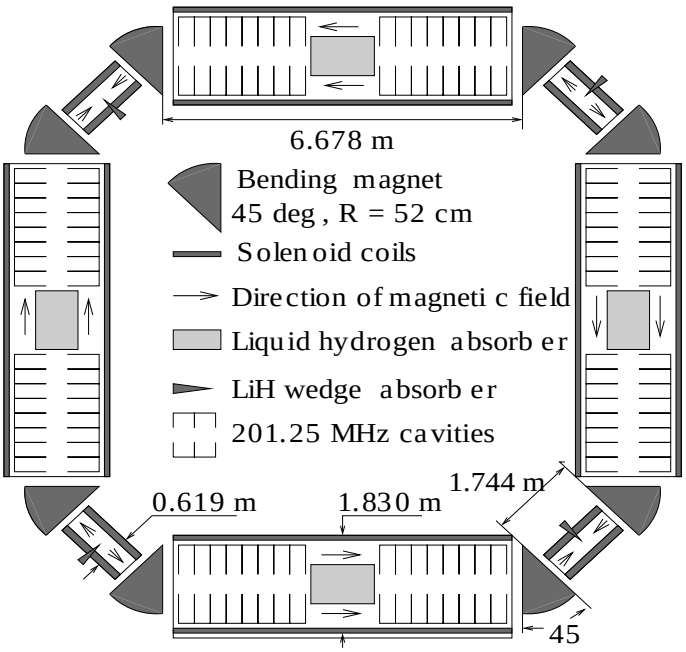

Figure 1: Layout of Balbekov ring [2].

The long straight section has a large solenoid surrounding RF cavities and a liquid hydrogen absorber for transverse cooling. The beam is bent in the short straight section by two gradient dipoles. In the center of the short straight section are two short solenoids with opposite field direction and a LiH wedge for emittance exchange.

2. Problem geometry

The model consists of a 4-sided ring with ~37 m circumference. Each quadrant of the ring is identical. The geometrical aspects of the elements in each quadrant are summarized in the following table.

Table 1: Geometry of ring quadrant

element	radius [m]	length [m]	Σ length [m]
drift	0.60	0.0720	0.072 0
RF1-8	0.57	8×0.32	2.632 0
drift	0.60	0.04	2.672 0
LH2	0.31	1.334	4.006 0
drift	0.60	0.04	4.046 0
RF9-16	0.57	8×0.32	6.606 0
drift	0.60	0.0720	6.678 0
dipole	0.52	0.408 4	7.086 4
drift + wedge	0.29	1.7439	8.830 3
dipole	0.52	0.408 4	9.238 7

LH2 refers to a cylindrical liquid hydrogen absorber.

3. Magnetic field modeling

The magnetic elements in the ring consist of solenoids and gradient dipoles. For the simulations shown in this report the fields of both the solenoids and dipoles end in a hard edge longitudinally.

3.1 Combined function dipole

The radius of the particle in the LAB coordinate system is

$$r = \rho + x$$

where ρ is the radius of curvature and the transverse coordinates (x,y) are measured relative to the reference trajectory. On the magnet midplane the vertical field is

$$B_{yo} = B_D \sqrt{\frac{1}{1+\frac{x}{\rho}}}$$

and the horizontal field vanishes. Define

$$w = y / r$$

Off the midplane the field is given is given by the expansions [3]

$$B_Y = B_{yo}\left[1-\frac{1}{8}w^2+\frac{25}{384}w^4-\frac{45}{1024}w^6+\frac{7605}{229376}w^8\right]$$

and

$$B_X = -B_{yo}\frac{w}{2}\left[1-\frac{5}{24}w^2+\frac{15}{128}w^4-\frac{585}{14336}w^6+\frac{14365}{458752}w^8\right]$$

The field is uniform along the longitudinal direction and ends abruptly at the hard edge.

3.2 Solenoid fringe fields

The effect of the fringe fields at the ends of the solenoids are approximated by transverse momentum kicks that are proportional to the radius of the particle. The symmetry of the kick orientation repeats twice each turn. Starting with a long straight section we used the series {- + - - + - + +}.

3.3 Long solenoid

The solenoids are modeled with current sheets. The parameters for the sheets used to model the long solenoid are given in the table.

Table 2: Current sheets for the long solenoid

#	z_o [m]	Length [m]	Radius [m]	J [A/mm^2]
1	-6.678	6.678	0.8275	43.79
2	-4.699	2.72	0.8625	43.79
3	-4.699	2.72	0.8975	43.79
4	0.	6.678	0.8275	43.79
5	1.979	2.72	0.8625	43.79
6	1.979	2.72	0.8975	43.79
7	6.678	6.678	0.8275	43.79
8	8.657	2.72	0.8625	43.79
9	8.657	2.72	0.8975	43.79

In the table the columns give the starting axial location of the sheet, the axial length of the sheet, the radius of the sheet and the current density in an equivalent current block with finite radial extent. In order to obtain the current gradient (A/m) required by the current sheets, it is necessary to normalize the current densities by an assumed 3.5 cm radial extent for the current blocks. The sheets 4-6 correspond to the actual current distribution in the ring. The preceding (1-3) and following (7-9) sheets produce the magnetic mirror ends assumed in the model. The resulting axial field component on-axis is shown in Fig. 2. The field starts at 2.08 T at the magnetic mirror and rises to 4.93 T at the center of the solenoid.

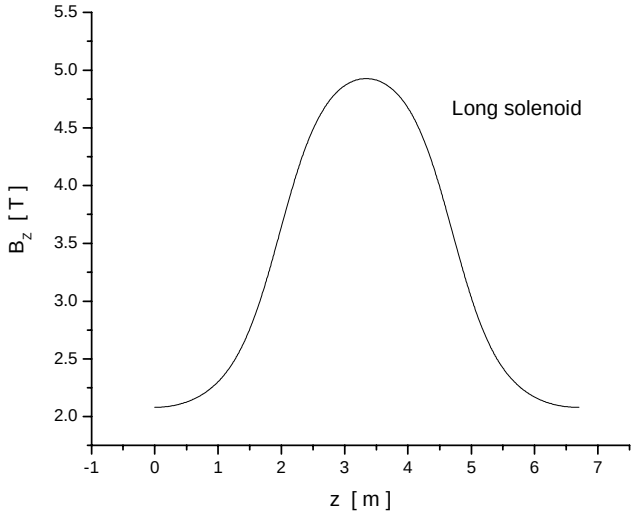

Figure 2: Axial magnetic field distribution for the long solenoid.

3.4 Field flip solenoids

The axial field changes direction between two short solenoids in the short straight section. The parameters for the sheets used to model this region are given in the table.

Table 3: Current sheets for the short straight section

#	z_o [m]	Length [m]	Radius [m]	J [A/mm^2]
1	-1.7439	0.4656	0.2972	-81.51
2	-1.2783	0.3816	0.2972	-203.78
3	-0.8472	0.3816	0.2972	203.78
4	-0.4656	0.4656	0.2972	81.51
5	0.	0.4656	0.2972	81.51
6	0.4656	0.3816	0.2972	203.78
7	0.8967	0.3816	0.2972	-203.78
8	1.2783	0.4656	0.2972	-81.51
9	1.7439	0.4656	0.2972	-81.51
10	2.2095	0.3816	0.2972	-203.78
11	2.6406	0.3816	0.2972	203.78
12	3.0222	0.4656	0.2972	81.51

Again only sheets 5-8 correspond to the physical coils, while the other sheets give the required magnetic mirrors at the ends. The axial field on-axis for the short straight section is shown in Fig. 3. The field starts at 2.08 T at the magnetic mirror and rises to 2.75 T and then falls to 0 at the center of the solenoid.

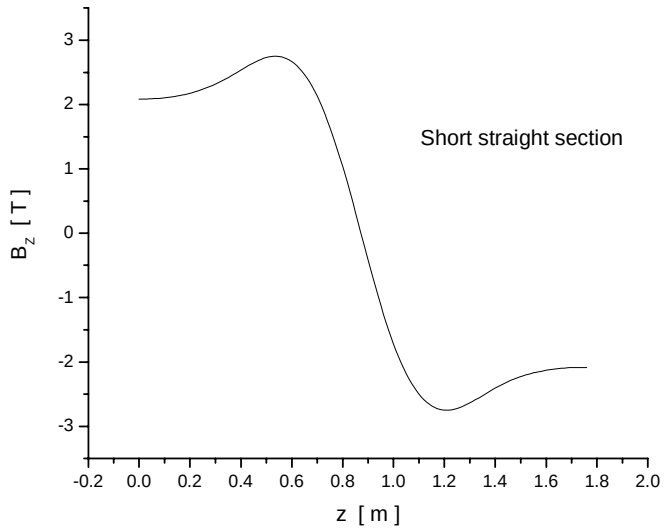

Figure 3: Axial magnetic field distribution for the short straight section.

4. Basic parameters for the ICOOL model

The ring contains 8 combined function dipoles with [2]

$B_D = 1.453$ T
$\rho = 0.52$ m
n = 1/2 (field index)

The dipole parameters fix the central momentum p_o and related quantities

$p_o = 0.226\ 511\ 190$ GeV/c

The bend angle of 45^o fixes the arclength in the dipole

$s_D = 0.408\ 4$ m

The revolution time around the ring depends on the detailed momentum profile of the reference particle. Starting at p_o the momentum will increase in the RF cavities in front of the hydrogen absorber, fall precipitously in the absorber, and then increase again back to p_o in the RF cavities after the absorber. However, we expect the average momentum over the whole path to be close to p_o . In that case the revolution time is

$T_{REV} \approx 136.020$ ns

For a harmonic number

h = 28

the corresponding RF period and frequency is

$T_{RF} = 4.857\ 85$ ns.
$f_{RF} = 205.852$ MHz

We took the length of liquid hydrogen absorber [2]

$L_{ABS} = 1.334$ m

The particles lose 40.27 MeV in the absorber.

The RF cavities are modeled as cylindrical pillbox cavities with Bessel function E_Z and B_φ field components. The cavity fields vary sinusoidally in time and have a length and peak on-axis gradient

$L_{CAV} = 0.32$ m
G = 15 MV/m

We checked the first-order dispersion suppression in the design by looking at a simplified system consisting only of the dipole-short solenoid-dipole combination [4]. For the first part of the study the wedge at the center of the solenoid was removed. On-axis particles were launched with momenta near p_o. We adjusted the overall current density scale factor in order to minimize the transverse beam position and momentum at the end of the simplified system. This optimization was not straightforward since for some solutions the particles were subsequently lost in multiturn tracking. The dynamics of the ring are strongly influenced by the exact design of this complicated field flip plus wedge region. The chosen solution produced a peak field of 2.75 T and a field at the solenoid hard edge of 2.08 T, in rough agreement with Fig. 3 in ref. [2]. Adjusting the two coil current densities in the field flipping short solenoid independently did not improve the results. The momentum region over which the dispersion-induced displacement is small is ~10 MeV, limited mainly by the dispersion in x.

We also used the dipole-short solenoid-dipole combination to check for proper operation of the LiH wedge. An on-axis beam was used with momentum spread σ_{PZ} = 18 MeV/c. The beam is dispersed in x by the first dipole. The solenoidal field between the dipole and the wedge rotates the dispersion so that it lies mainly in the y direction going into the wedge. The wedge properties were

$\alpha_W = 25.4^o$
width = 29 cm
thickness = 13.07 cm

The wedge is oriented vertically with the apex touching the beam axis. We found that, as desired, the average energy and the energy spread are reduced in one half of the vertical dimension and left alone in the other half.

A discussion of the design considerations for this ring, together with the theoretical lattice functions and resonance behavior can be found in a recent paper by Balbekov [5]. Some further details about the longitudinal dynamics of the ring are given in the appendix of this report.

5. Reference particle

ICOOL uses an internal reference particle to set the absolute phases of the RF cavities. The algorithm chosen here (phase model 3) starts with an on-axis particle with momentum p_o and all stochastic processes turned off. It is assumed that the reference particle moves with constant momentum p_o. The time and axial position are simply updated for non-cavity regions. For RF cavity regions the time the reference particle reaches the center of the cavity is stored and used to define the zero-crossing time of the cavity electric field. Since the harmonic number is an exact integer, this model for the reference particle essentially gives a timing pulse that periodically drives the sinusoidal fields in the RF cavities.

Once the absolute cavity phases have been fixed we can look at tracking real particles. We assume that the cavities in the other three quadrants of the ring have the same absolute phase as the corresponding cavity in the first quadrant. We start with a particle with momentum p_o. In order for the particle to get accelerated in the cavities, we shift its launch time by -0.473 ns relative to the reference particle. The particle phase crossing the cavities is then just right to end up with momentum p_o after leaving the 16th RF cavity. This corresponds to a synchronous phase of 35.0^o from zero-crossing.

However, there is a time shift between the real particle and the reference particle when entering the first dipole. This means the real particle will enter the first cavity in the next quadrant at a different phase than it entered the first cavity in the first quadrant. As a result all the real particles undergo synchrotron oscillations in longitudinal phase space. This time difference comes about because the real particle does not have the same momentum profile through the cavities and absorbers that was assumed for the reference particle. However, this algorithm gives a phase stable solution. This can be seen in Fig. 4, which shows the longitudinal momentum of the real particle as a function of distance.

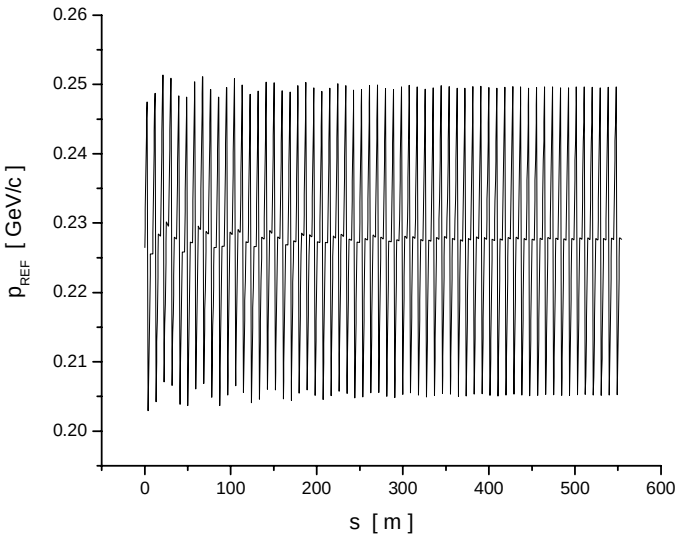

Figure 4: Axial momentum of a real reference particle as a function of distance.

6. Initial beam conditions

The initial beam distributions given in Table 4 differ from those given in ref. [2] because we started the simulation at a location between one of the dipoles and a long straight section, whereas the Balbekov simulation began in the middle of the long straight section.

The initial beam was given a transverse amplitude-momentum correlation according to the following prescription [5]. Let us define the square of the Balbekov amplitude

$$A_B^2 = \left(\frac{p_T}{mc} \right)^2 + \left(\frac{eBr}{2mc^2} \right)^2$$

The quantities {r, p_T} are randomly chosen to determine the initial value of this amplitude. The quantity B is the value of the solenoidal magnetic field at the launch location for the particles. Once A_B is known, we set the total energy of the particle according to

$$E = E_{REF} \sqrt{1 + A_B^{\ 2}} + \Delta E$$

The quantity E_{REF} is fixed at 250 MeV, as in ref. [2], and ΔE was selected randomly. Fig.5 shows the resulting correlation of total energy versus the Balbekov amplitude when ΔE=0.

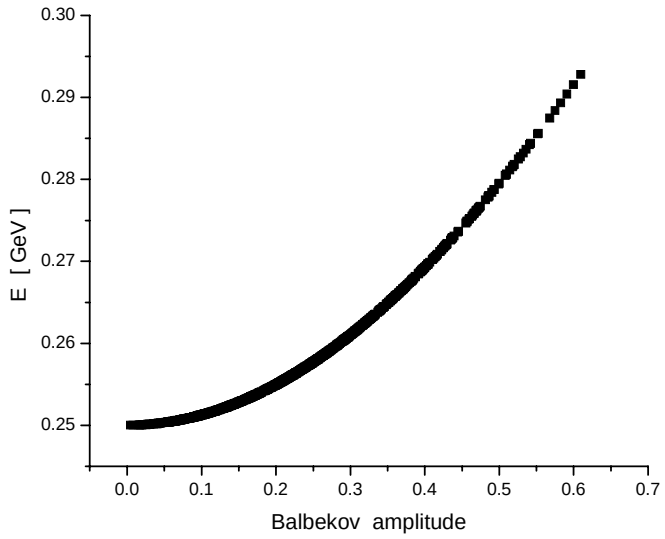

Figure 5: Transverse amplitude-momentum correlation of initial beam particles.

7. Full beam simulations

We have simulated propagation through 15 complete turns, including all stochastic effects. The widths of the beam parameter distributions at the beginning and end of the simulation are given in Table 4.

Table 4: Initial and final beam standard deviations

σ		Initial	Final
x	mm	61.7	24.1
y	mm	63.3	23.7
ct	mm	98.8	55.3
p_X	MeV/c	20.6	8.36
p_Y	MeV/c	20.4	7.57
p_Z	MeV/c	22.1	9.85

Fig. 6-8 shows the standard deviations of the beam distributions as a function of axial distance.

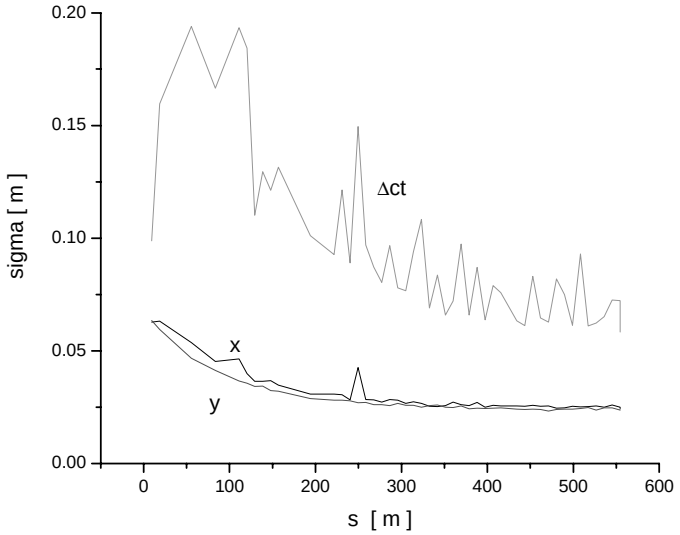

Figure 6: Standard deviation of beam dimensions as a function of axial distance.

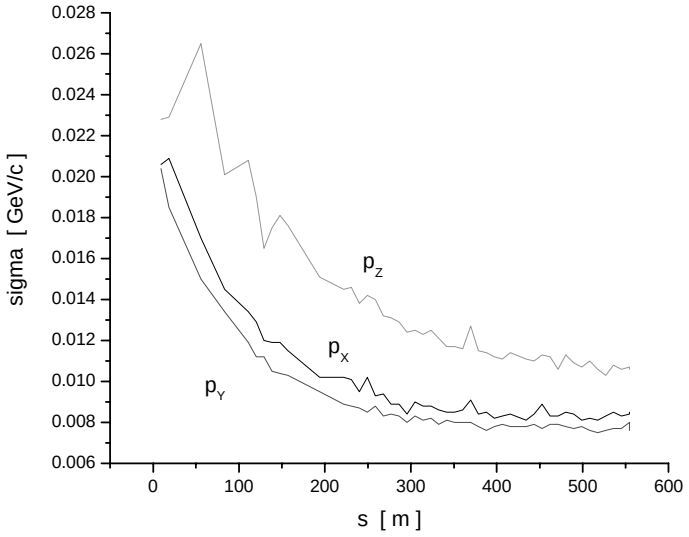

Figure 7: Standard deviation of beam momenta as a function of axial distance.

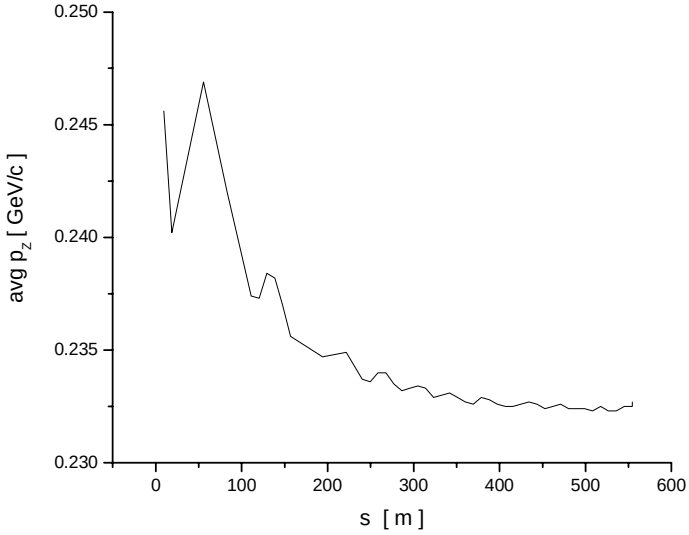

Figure 8: Mean of beam momenta as a function of axial distance.

We see that the beam size is steadily reduced in all six phase space dimensions. Fig. 8 shows that the mean momentum of the muon bunch decreases gradually as the cooling takes place.

Fig. 9 shows the longitudinal phase space after 15 turns. We see that the beam has been successfully captured in an rf bucket.

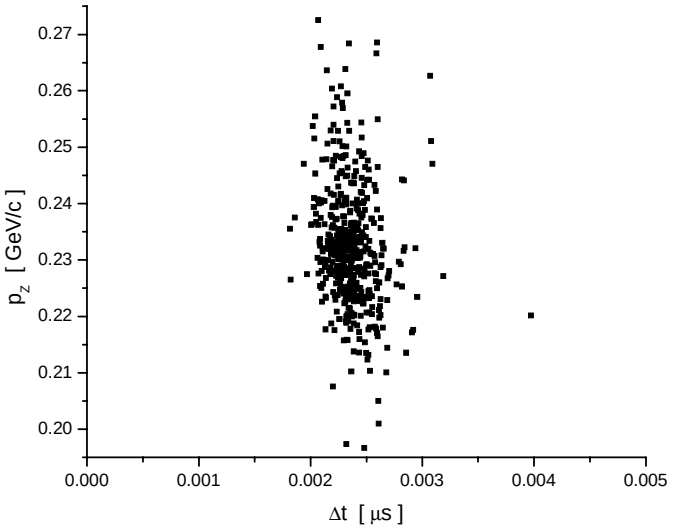

Figure 9: Longitudinal phase space at end of 15 turns.

Fig. 10 shows the normalized emittances computed using the program ECALC9 and transmission including decay as a function of distance for 15 complete turns around the ring.

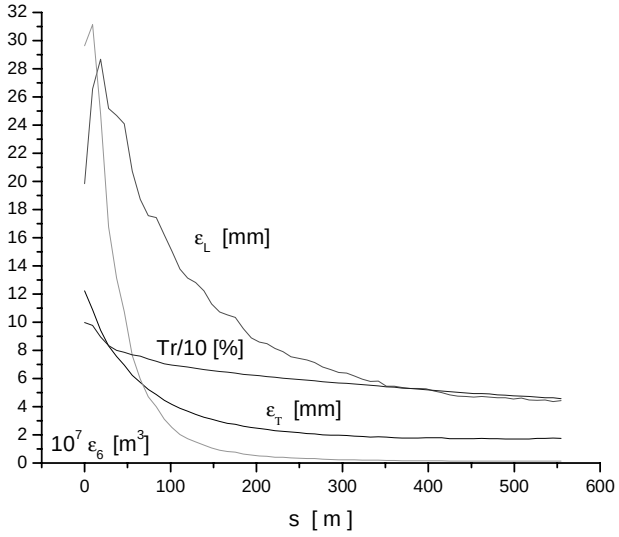

Figure 10 Emittances and transmission at end of 15 turns.

The transverse emittance falls monotonicly from the beginning. The longitudinal and 6D emittances on the other hand grow significantly in the first turn, then begin to fall steadily as well. The transmission also has a rapid drop in the first turn as mismatched particles are lost due to scraping at the transverse apertures. The emittance values at the beginning and end of the simulation are given quantitatively in Table 5.

Table 5: Initial and final beam emittances

		initial	final
ε_T	mm	12.2	1.74
ε_L	mm	19.9	4.44
ε_6	10^{-9} m^3	2960	13.2
Tr	%	100	45.8

The ring brings the transverse normalized emittance down to ~1.7 mm and the longitudinal normalized emittance down to ~4.5 mm.

The merit functions [6] are shown as a function of distance in Fig. 11.

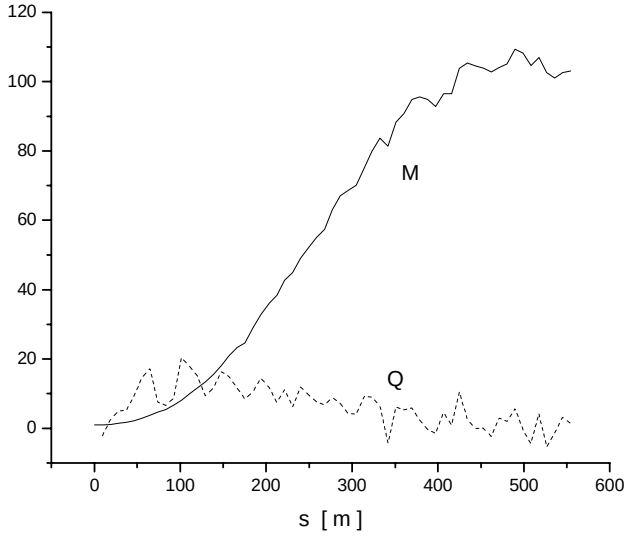

Figure 11 Merit factors M and Q as a function of axial distance.

The ring gives a peak merit factor of 109 after 490 m and then decreases slightly to a value of 103 after 15 complete turns. If the emittances are corrected for the transverse amplitude-momentum correlation, this drops to 97. A simulation done without the initial transverse-longitudinal correlation in the beam gave a final merit factor of 51.

7. Conclusions

The simulation of the ring given here agrees qualitatively with the results obtained by Balbekov using his own code. The predicted merit factor ~103 in ICOOL is more than two times better than that predicted by Balbekov. There are several possible explanations for this difference in simulated behavior. There are small differences in the reoptimized parameters used here. Perhaps more significantly the initial longitudinal momentum determined here is larger than the one assumed in ref. [5], which leads to a higher merit factor. Nevertheless there is no doubt that a ring with parameters similar to those assumed here would work well. The major issue lies with these assumptions. The hard-edge field approximations used in both simulations is clearly inadequate. The next step in the study of this ring must be to drop the hard-edge field approximation and reoptimize the ring using realistic fields, including the effects of overlapping fields from the solenoids and dipoles. In addition the ring design assumed here does not allow breaking the lattice symmetry for an injection/extraction region. Early attempts at including such a section led to seriously degraded cooling performance [5].

Acknowledgements

The would like to thank Valeri Balbekov, Rajendran Raja, and Zafar Usubov for useful discussions about the properties of this ring.

Notes and references

[1] V. Balbekov & A. Van Ginneken, Ring cooler for muon colllider, in D. Cline (ed), Physics Potential and Development of μ μ Colliders, AIP Conf. Proc. 441, 1998, p. 310-3.

[2] V. Balbekov et al, Muon ring cooler for the MUCOOL experiment, Proc. 2001 Part. Acc. Conf., Chicago, IL, p. 3867-9.

[3] The coefficients of these expansions were taken from the Geant parameter file mucool.rcp in Oct. 2001.

[4] R.C. Fernow, Status report on modeling the Balbekov square ring in ICOOL, http://www.fnal.gov/projects/muon_collider/eexchange/Meetings/Meeting3/fernow.pdf

[5] V. Balbekov, Ring cooler progress, MC collaboration note MUC-NOTE-COOL_THEORY-246, May 2002.

[6] R.B. Palmer, Cooling efficiency factor, MC collaboration note MUC-NOTE-COOL_THEORY-250, July 2002.

[7] A. Chao & M. Tigner, Handbook of Accelerator Physics and Engineering, World Scientific, 1999, p. 50-1.

[8] D. Neuffer, Calculations of predicted performance for μ-cooling rings, MC collaboration note MUC-NOTE-COOL_THEORY-227, 2001.

Appendix: Ring behavior for off-momentum particles

Several properties of the ring can be determined from tracking particles with momentum unequal to p_o through a single turn. The compaction factor is [7]

$$\alpha_p = \frac{\frac{\Delta C}{C}}{\frac{\Delta p}{p_o}}$$

The transition gamma is [7]

$$\gamma_t = \frac{1}{\sqrt{\alpha_p}}$$

The slip factor is [7]

$$\eta = \frac{1}{\gamma_t^2} - \frac{1}{\gamma_o^2}$$

We find

$\alpha_p = 1.223\ 10^{-3}$
$\gamma_t = 28.590$
$|\eta| = 0.177$

The longitudinal beta function is [8]

$$\beta_\phi^2 = \frac{1}{\beta^3 \gamma e V' \cos(\phi_s)} \frac{2\pi}{\lambda_{RF}} \frac{\eta}{mc^2}$$

where our synchronous phase is measured from zero-crossing. We find

$\beta_\phi = 0.0181\ \text{MeV}^{-1}$

By observing the counter-clockwise rotation of the bunch in longitudinal phase space, we determined that the synchrotron wavelength is approximately the same as the circumference of the ring (~37 m).